Supplementary Information for: Electronic properties of single-layer tungsten disulfide on epitaxial graphene on silicon carbide

Stiven Forti,*[a] Antonio Rossi,[a,b] Holger Büch,[a] Tommaso Cavallucci,[b] Francesco Bisio,[c] Alessandro Sala,[d] Tevfik Onur Menteş,[d] Andrea Locatelli,[d] Michele Magnozzi,[e] Maurizio Canepa,[e] Kathrin Müller,[f] Stefan Link,[f] Ulrich Starke,[f] Valentina Tozzini[b] and Camilla Coletti[a,g]

1 Model systems and DFT calculations

Two different series of DFT calculations were performed: one with the unit cell of WS_2 and one for the graphene plus WS_2 system using the consensus supercell, namely the (9×9) for graphene and the (7×7) for WS_2, which includes 162+147=309 atoms. The initial thickness of the graphene-WS_2 system is 8.40 Å (distance between the graphene layer and the top of the WS_2 layer), which corresponds to the upper limit suggested by the experimental measurement. All cells and their Brillouin zones are reported in Fig. S1, with the relative location of symmetry points. The cell parameters used are reported in Table 1.

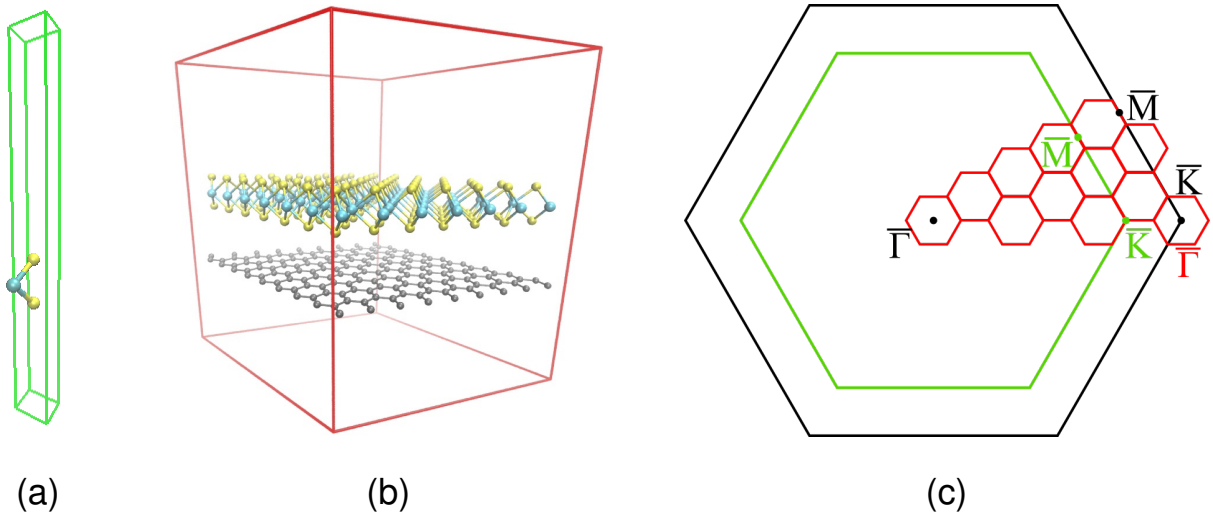

Figure S1 (a) WS_2 unit cell and (b) graphene-WS_2 supercell used in calculations: cell boundaries in green (unit cell) and red (supercell), structures in ball and stick representation (C = grey, S = yellow and W = cyan). (c) Brillouin zones of graphene (black), of WS_2 (green) and of the supercell (red), with symmetry points reported. As it can be seen upon refolding, the $\overline{K}$ point of the graphene unit cell is remapped onto the $\overline{\Gamma}$ point of the consensus supercell.

To speed up calculations, we used ultrasoft[1] RRKJ[2] pseudopotentials combined with a PBEsol[3] functional, scalar relativistic for collinear calculations and fully relativistic for spin-orbit calculations. Van der Waals (vdW) corrections were included according to the Grimme scheme[4]. Convergence checks on energy were performed using the WS_2 unit cell (see Fig. S2(a) and S2(b)). A good convergence is achieved at 30 Ry. The density cutoff was set 10 times larger than the wavefunction cutoff in any case. The convergence vs. the k point sampling was also tested (Fig. S2(c) and S2(d)). The final choice was to use a $15\times15\times1$ grid for the unit cell. For the complete system we performed $\overline{\Gamma}$ point calculations, which were proven sufficient for structure convergence in

[a] *Center for Nanotechnology Innovation @ NEST, Istituto Italiano di Tecnologia, Piazza San Silvestro 12, 56127 Pisa, Italy; E-mail: stiven.forti@iit.it*
[b] *NEST, Istituto Nanoscienze-CNR and Scuola Normale Superiore, Piazza S. Silvestro 12, 56127 Pisa (Italy)*
[c] *CNR-SPIN, Corso F. Perrone 24, 16152 Genova, Italy*
[d] *Elettra - Sincrotrone Trieste S.C.p.A., Basovizza, Trieste 34149, Italy*
[e] *OPTMATLAB and Dipartimento di Fisica, Universitá degli Studi di Genova, via Dodecaneso 33 16146, Genova, Italy*
[f] *Max-Planck-Institut für Festkörperforschung, Heisenbergstr. 1, D-70569 Stuttgart*
[g] *Graphene Labs, Istituto Italiano di Tecnologia, via Morego 30, 16163 Genova, Italy*

Table 1 Calculation setup and parameters for the WS_2 unit cell and for the graphene-WS_2 system

	WS_2 unit cell	**Consensus supercell**
a (Å)	3.16	22.14
c (Å)	25.0	30.0
Atoms	3	309
k-points (scf)	$15 \times 15 \times 1$	Γ
Sampling for band calculation (MΓKM)	200	72
Gaussian smearing (Ry)	0.01	0.01
Convergence threshold	10^{-8}	10^{-8}
Spin treatment	Collinear Spin-orbit coupling	Collinear

our previous calculations for smaller supercells[5]. The band structure was evaluated on a sufficiently dense set of points along the main symmetry directions. In order to compare the isolated WS_2 bands with those of the combined system and with the experiment, an unfolding procedure was applied to the band calculations of the latter, using the method developed by Popescu and Zunger[6]. For each supercell state, defined by k point and band index, the spectral weight, namely the probability of finding a set of states of the unit cell contributing to the supercell state, is calculated. Then for each point in the unit cell k-energy space, the spectral function is calculated averaging the contribution of all supercell k points that belong to the same symmetry class. This yields a blurred plot of the band structure. The code used is part of the Quantum ESPRESSO project[7]. The remapping of points upon refolding is illustrated in Fig. S1(c).

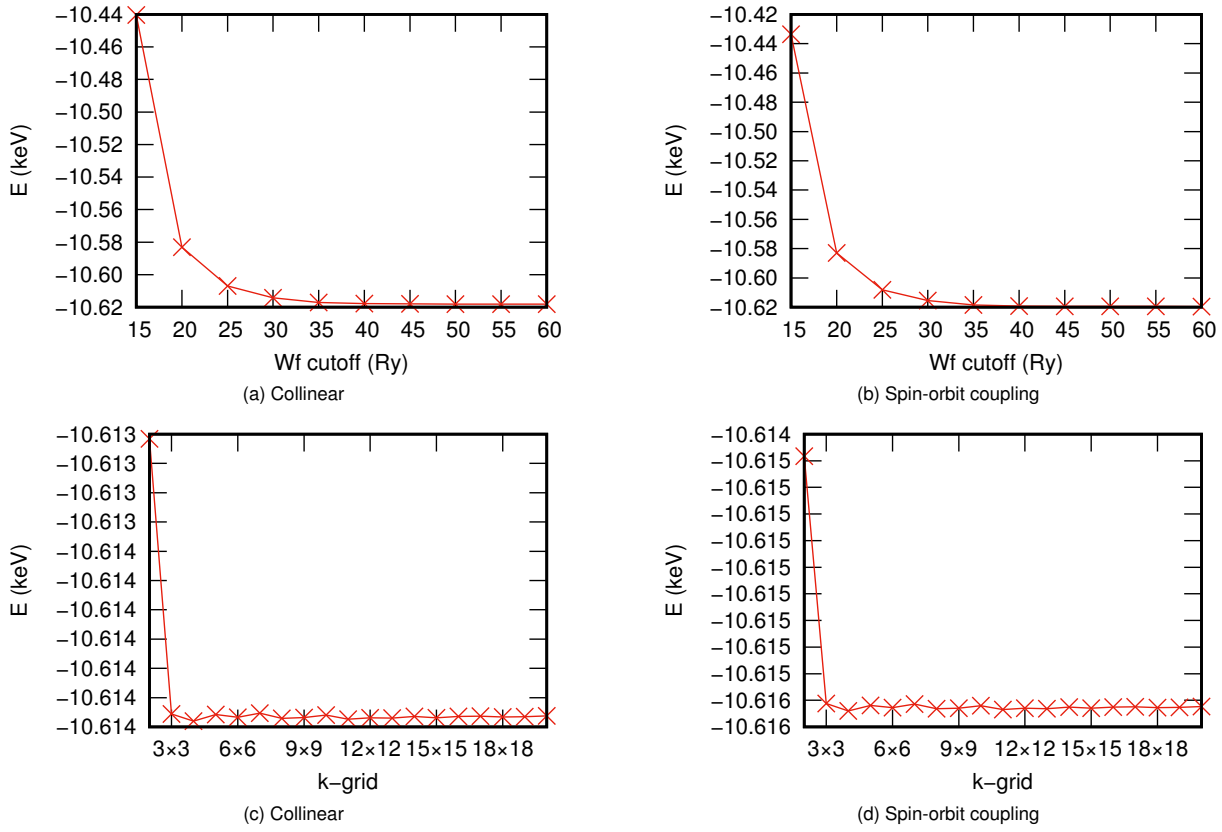

Figure S2 Wave function cutoff energies and k-grids for the collinear and spin-orbit pseudopotentials. Each plot shows the total energy as a function of (a)-(b) the wave function cutoff energy and (c)-(d) the reciprocal space sampling. The total energy depends on the pseudopotential used, hence it does not have a straight physical meaning and values from collinear and spin-orbit calculations can not be directly compared.

Beside the neutral supercell system, the n-doped system was studied to emulate the polarization effect of the SiC substrate. A negative charge of 0.5 electrons per supercell, corresponding to $\sim 10^{13}$ cm^{-2} and a shift of 15 meV of the Dirac point and 122 meV of the WS_2 bands, was added to the cell, while a compensating positive background charge was added to restore charge neutrality.

2 Calculations results

Structural optimization was performed both without and with the vdW corrections, with convergence thresholds of 10^{-3} a.u. for forces and 10^{-4} Ry for the total energy. For the unit cell, the relaxed WS_2 layer has a thickness of 3.12 Å and the W-S bond length is equal to 2.40 Å. The graphene-WS_2 relaxation gives almost the same thickness of the WS_2 layer (3.11 Å) and a negligible change in the bond lengths (within 10^{-3} Å). However, the system thickness depends on the vdW corrections: when they are present. The optimized graphene-WS_2 distance is 3.14 Å from graphene to the bottom of WS_2 and 6.25 Å to the upper side of the WS_2 layer, while in absence of vdW corrections, the configuration remains basically the starting one, namely with 5.11 Å of interlayer distance and 8.35 Å of total thickness. WS_2 and graphene layer energies were also calculated separately, with the same structures of the relaxed full system, in order to evaluate the van der Waals interaction energy between the layers, which results to ∼240 meV per superficial S atom (i.e. half of the supercell S atoms), or equivalently ∼72 meV per C atom with vdW corrections. The van der Waals interaction energy evaluated in the experimental structure is lower, namely ∼50 meV per superficial S atom and ∼15 meV per C atom.

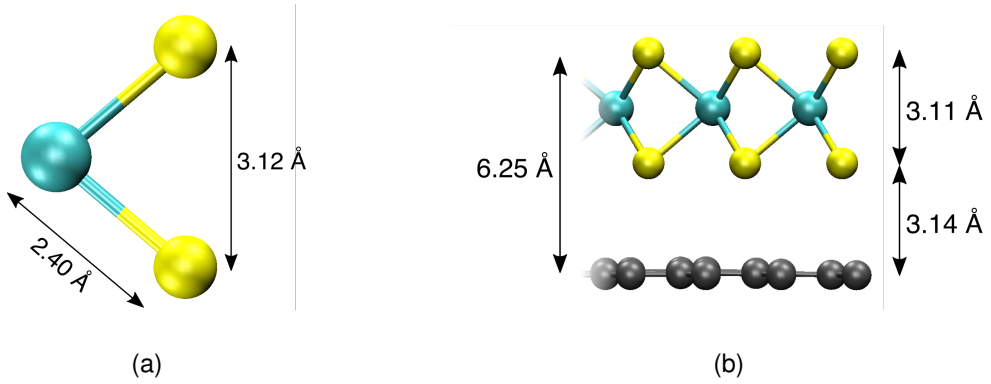

Figure S3 Relaxed structured and main distances of (a) WS_2 unit cell and (b) graphene-WS_2 supercell with vdW corrections.

The band structure was evaluated in the isolated WS_2 unit cell and in the interacting graphene-WS_2 system, in the neutral and doped, vdW corrected and uncorrected system. The band structure of all the evaluated cases is reported in Fig. S4. The comparison between the bands without vdW correction and larger thickness (Fig. S4(a)) and those with corrections and smaller thickness (Fig. S4(c)) shows an average ∼0.4 eV upward shift of the filled band system and ∼0.6 eV of the empty bands, and a ∼4 meV gap opening at the $\overline{K}$-point which can be attributed to the stronger interaction between the two layers in the latter configuration. The additional doping (Fig. S4(e)) produces a shift of the Dirac point of 15 meV (inset in Fig. S4(e)). Fig. S4(b), S4(d) and S4(f) show that the increased van der Waals interaction produces an upward shift of ∼120 meV of the WS_2 bands with respect to the graphene bands, while the effect of doping seems negligible.

2.1 Orbital character of the valence band

In this section we show the projection of the WS_2 wave functions onto the different p and d orbitals along the high-symmetry paths in k-space to highlight the orbital character of the valence band as a function of k. The composition of the electronic states of the WS_2 unit cell (modelled without substrate) was also analyzed by projecting the wave functions $\psi_\nu(\vec{k})$ onto the atomic orbitals (evaluated with the same DFT calculation setup). The projection along each band $E(\vec{k})$ is

$$P_i(\vec{k},E) = \sum_{\nu}^{\text{bands}} \sum_{j} c^*_{j\nu}(\vec{k}) c_{i\nu}(\vec{k}) S_{ij}(\vec{k}) \delta\left(E - E_\nu(\vec{k})\right) \quad ,$$

i being the atomic orbital index, $c_{i\nu}(\vec{k})$ the expansion coefficient of the electronic state onto the atomic orbital basis and S_{ij} the overlap matrix between atomic orbitals. The atomic orbitals are 17 for W (namely two s states, three p states, five d states and seven f states) and 8 for S (the 3s and the 3p states for each of the two S atoms). In the plot, the following combinations are reported, obtained summing contributions with given symmetry with respect to the z axis

- $d_{x^2-y^2} + d_{xy}$: sum of W d orbitals with $m = -2$ and $m = 2$.

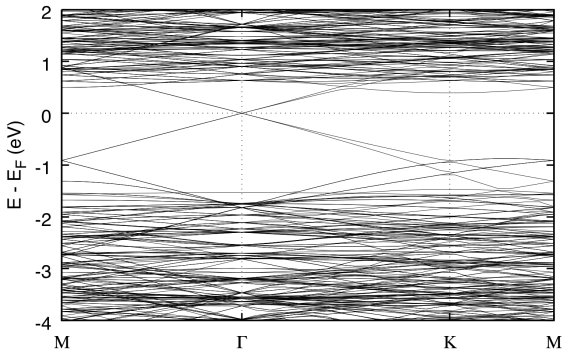

(a) Without vdW correction (experimental distance)

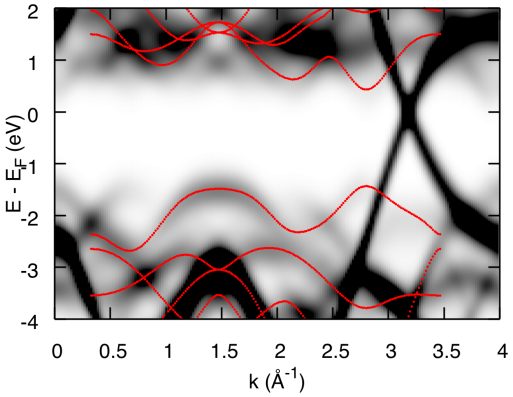

(b) Without vdW correction, unfolded

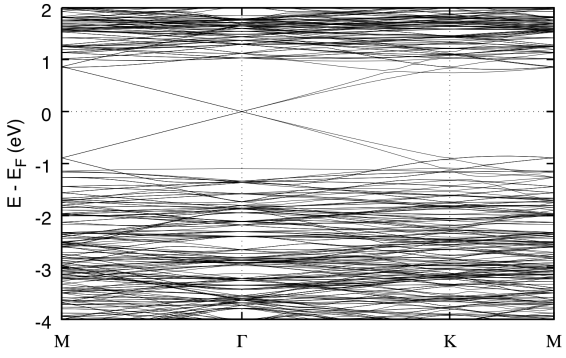

(c) With vdW correction (DFT optimized structure)

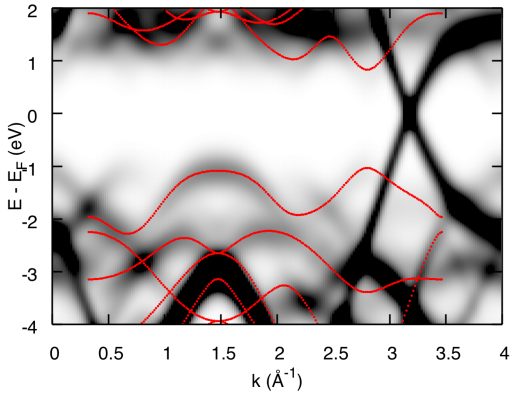

(d) With vdW correction, unfolded

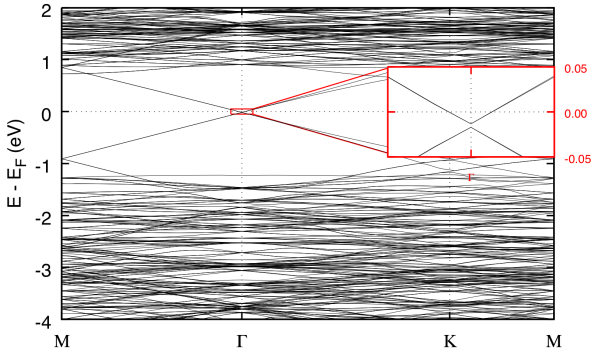

(e) n doped with vdW correction (DFT optimized structure)

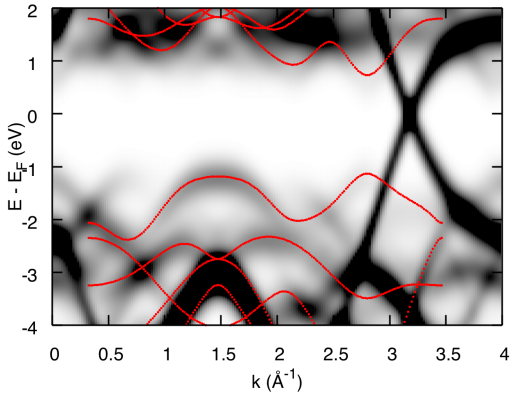

(f) n doped with vdW correction, unfolded

Figure S4 Energy bands of the different models: (a)-(b) optimized without vdW corrections, (c)-(d) optimized with vdW corrections and (e)-(f) with doping. Bands (a)-(c)-(e) are the consensus supercell, while (b)-(d)-(f) are those obtained upon unfolding to compare with experiment. The bands of the WS_2 unit cell are superimposed as red lines, manually aligned to the unfolded interacting system top of valence band of gamma point located at 1.47 $Å^{-1}$.

- $d_{xz}+d_{yz}$: sum of W d orbitals with $m=-1$ and $m=1$.
- d_{z^2}: W d orbital with $m=0$.
- $p_{x,y}$: sum of W and S orbitals with $m=-1$ and $m=1$.
- p_z: sum of W and S orbitals with $m=0$.

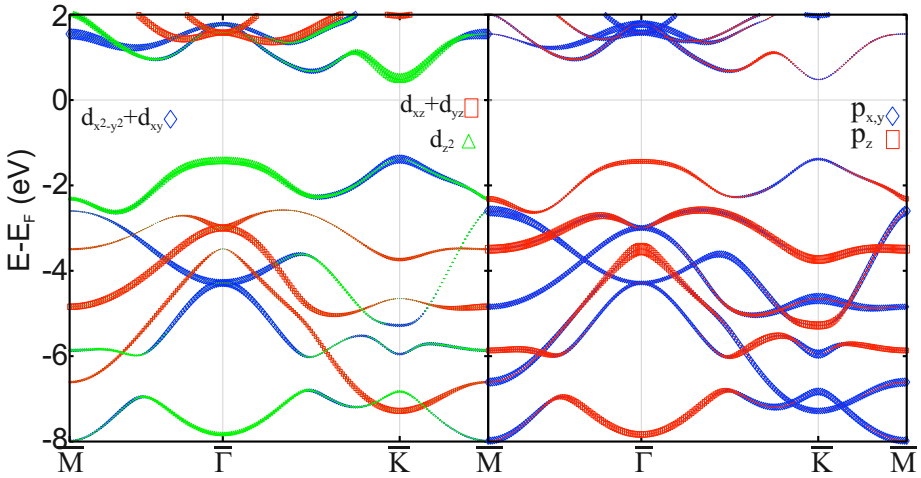

Figure S5 d (left) and p (right) composition of electronic states of WS_2 (unit cell) atomic orbitals, evaluated as specified in the text. The size of symbols is proportional to the numerical value of projection.

3 ARPES raw data

In this section we show the ARPES spectra of Fig. 2 without the superposition of calculated bands. Fig. S6(a) is

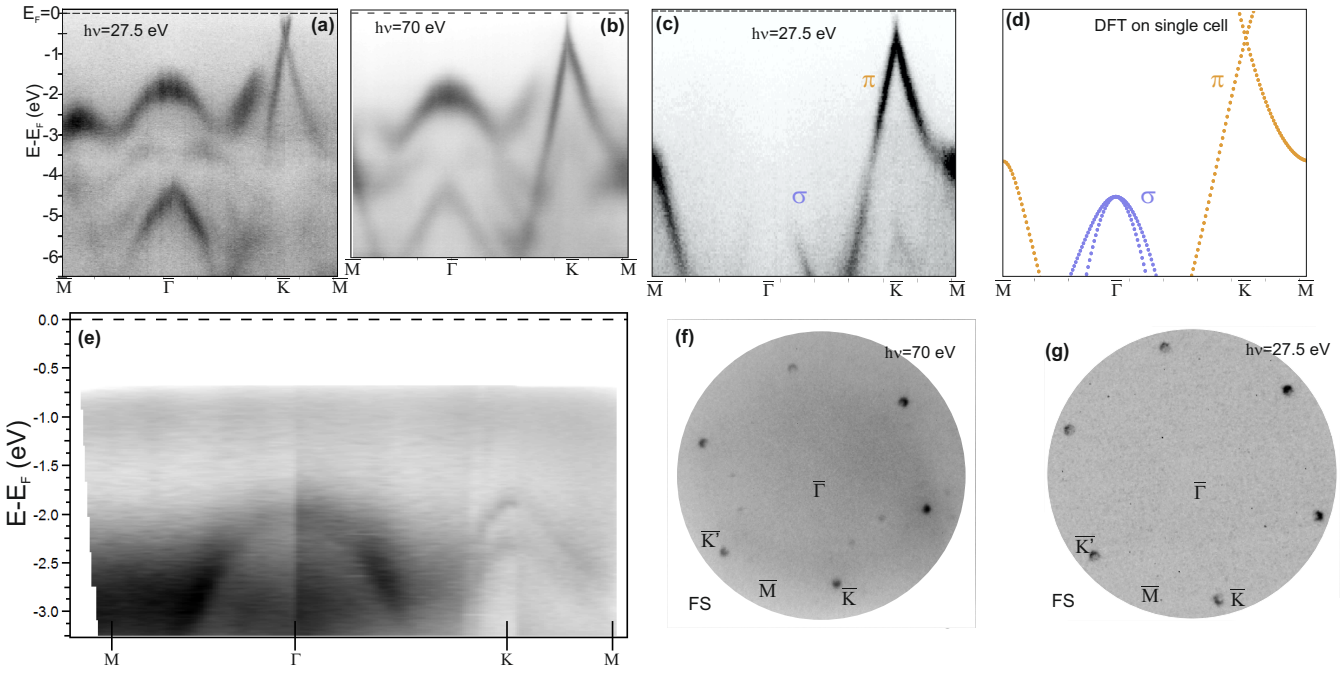

Figure S6 μ-ARPES measured on single-crystal WS_2/graphene/SiC(0001) with photon energy 27.5 eV (a) and 70 eV (b). The high symmetry points refer to the graphene's BZ. (c) Measured μ-ARPES on MLG at 27.5 eV. (d) Single u.c. DFT calculated bands. (e) ARPES data acquired with the laboratory setup at the MPI in Stuttgart. Here, the high symmetry points of the WS_2 BZ are indicated. (f) and (g) Fermi surface extracted from the μ-ARPES data at 70 eV (f) and 27.5 eV (g).

the same as Fig. 3(a). The high symmetry points used as labels for panels (a,b,f,g) refer to the graphene's BZ. In panel (c), the graphene's π-bands μARPES measurement at 27.5 eV is shown. In panel (d) the DFT bands calculated over the single graphene u.c. are shown. Panel (e) correspond to the raw ARPES data shown in Fig. 2(e), acquired with the laboratory setup at the MPI in Stuttgart (see section 2.1 in the paper for details). Panels (f) and (g) are the Fermi surface recorded with μARPES on a WS_2/MLG crystal for photon energy 70 eV and 27.5 eV, respectively. In panel (f) graphene replica bands are visible. The reciprocal lattice vectors that generate those replicas are the well known 1/6 of SiC $(6\sqrt{3}\times 6\sqrt{3})$R30° reconstruction and the WS_2 (10) vector.

4 WS_2 spin-orbit splitting in $\overline{K}$

In this section we show the ARPES single spectrum measured in $\overline{K}$ as indicated in the inset of Fig. S7 with He I light. On the right side of the panel, the line intensity profile of the spectrum is shown. The profile is obtained

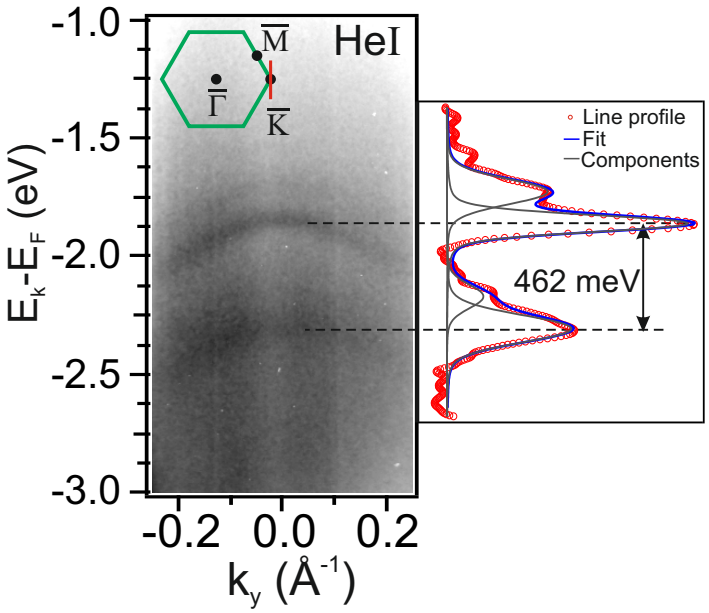

Figure S7 ARPES spectrum of WS_2 bands measured in $\overline{K}$ along the red line in the inset with He I light. On the side, intensity line profile obtained integrating the spectrum through zero with a line profile thickness of 0.05 Å^{-1}.

by integrating the intensity of the spectrum about zero, on a region of ± 0.025 Å^{-1}. The line profile was fitted with four Voigt components. The two at lower binding energies are attributed to bilayer WS_2, as also visible from Fig. 1(b).

5 X-Ray Photoelectron Spectroscopy Data

This section is aimed to show the laterally averaged photoelectron spectroscopy data, acquired with a Al-K$_\alpha$ source as described in the 2.1 section in the main text with a photon beam spot of 2×3 mm^2 in size. The C 1s

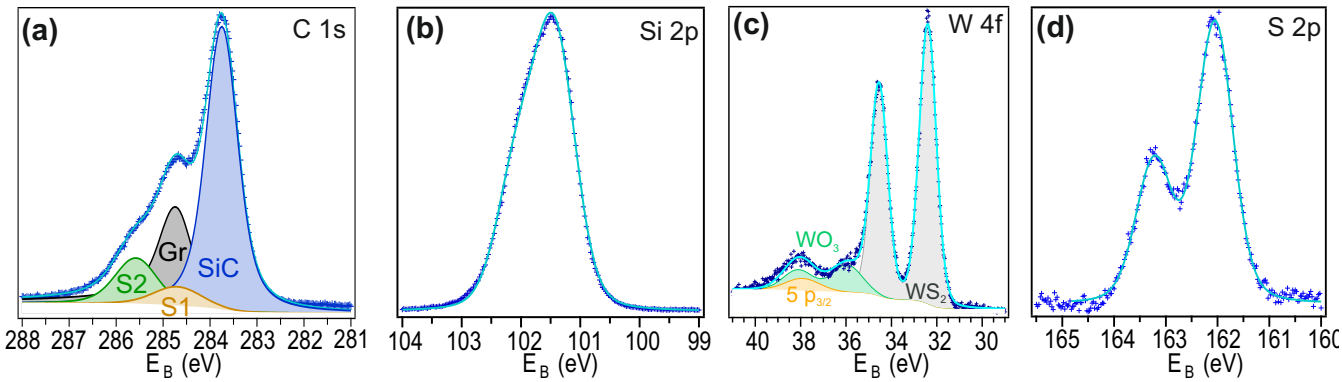

Figure S8 XPS spectra recorded at room temperature on a Kratos Al-Kα laboratory system.

and Si 2p spectra (panels (a) and (b), respectively) do not show any peculiar feature deviating from the results expected from a MLG/SiC(0001). The W 4f peak confirms the XPEEM measurements shown in Fig.4(e) of the main text. Here, the WO_3/WS_2 components ratio is slightly higher, indicating a possible inhomogeneity in the WO_3 concentration throughout the sample. Given the higher surface sensitivity of the XPEEM at lower photon energies compared with the XPS, it could also indicate that the WO_3 is actually underneath the WS_2 and not on top. However, its contribution remains very little. The sulphur component was fitted with a single Voigt doublet in this case as well, as it was the XPEEM peak shown in Fig.4(d).

6 Overview on the growth of WS_2 on epitaxial graphene

The growth of WS_2 on graphene is a reliable and reproducible technique. It depends critically on the reagents ratio, carrier gas flux (Ar in our case), temperature and distance substrate-WO_3 as described in Ref. [8, 9]. In particular we observe that the WS_2 coverage with respect the graphene area decreases turning away the substrate from the WO_3 powder. Moreover an over sulfurized environment ensures to avoid the formation of any unwanted byproduct such as WO_2, which forms 3D cluster. Therefore the optimal ration WO_3:S is 1:100. When byproducts are taken into account also the Ar flux is important since only a sufficient high vapor pressure enables mixing of atomic gases in the right stoichiometry, which are subsequently transported to the substrate. However, the total built-in pressure in the chamber influences the nucleation density. In particular passing from 0.5 to 5 mbar, we can distinguish a higher and a lower nucleation density respectively. The first leading to a continuous large-scale polycrystalline sub-μm size epitaxial film and the second to a $\sim \mu$m size well isolated crystals. Temperature is another parameter that limits the reaction process. If the temperature is too low a polycrystalline film with sub-μmeter grain size will form since adatoms will not have enough kinetic energy to diffuse and find the lowest potential energy site. On the other hand if it is too high the surface diffusion will be fast enough to let molecules deposit on o the energetically most favorable places and results in a 3D island growth, or in the worst case leading to the desorption of the molecules from the substrate.

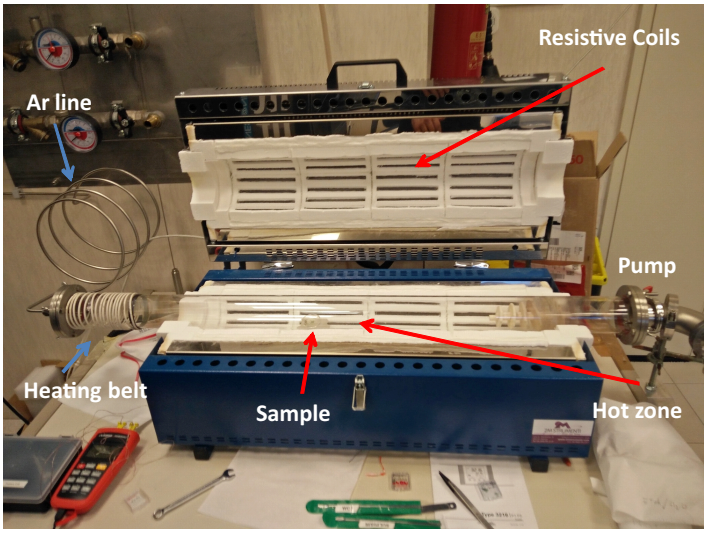

Figure S9 Picture of the oven and reactor used for the growth. Main parts are indicated with arrows.

References

[1] D. Vanderbilt, *Phys. Rev. B*, 1990, **41**, 7892.

[2] A. M. Rappe, K. M. Rabe, E. Kaxiras and J. Joannopoulos, *Phys. Rev. B*, 1990, **41**, 1227.

[3] J. P. Perdew, A. Ruzsinszky, G. I. Csonka, O. A. Vydrov, G. E. Scuseria, L. A. Constantin, X. Zhou and K. Burke, *Phys. Rev. Lett.*, 2008, **100**, 136406.

[4] S. Grimme, *J. Comp. Chem.*, 2006, **27**, 1787–1799.

[5] A. Rossi, S. Piccinin, V. Pellegrini, S. de Gironcoli and V. Tozzini, *J. Phys. Chem. C*, 2015, **119**, 7900–7910.

[6] V. Popescu and A. Zunger, *Phys. Rev. B*, 2012, **85**, 085201.

[7] P. Giannozzi, S. Baroni, N. Bonini, M. Calandra, R. Car, C. Cavazzoni, D. Ceresoli, G. L. Chiarotti, M. Cococcioni, I. Dabo, A. D. Corso, S. de Gironcoli, S. Fabris, G. Fratesi, R. Gebauer, U. Gerstmann, C. Gougoussis, A. Kokalj, M. Lazzeri, L. Martin-Samos, N. Marzari, F. Mauri, R. Mazzarello, S. Paolini, A. Pasquarello, L. Paulatto, C. Sbraccia, S. Scandolo, G. Sclauzero, A. P. Seitsonen, A. Smogunov, P. Umari and R. M. Wentzcovitch, *J. Phys.: Condens. Matter*, 2009, **21**, 395502.

[8] P. Solìs-Fernández, M. Bissett and H. Ago, *Chem. Soc. Rev.*, 2017, **46**, 4572.

[9] W. Choi, N. Choudhary, H. H. Gang, J. Park, D. Akinwande and Y. H. Lee, *Mater. Today.*, 2017, **20**, 116.